

Optimization sealing and cooling to control gas intrusion in a floating-wall combustion chamber

Hong SHI¹ , Rui WANG¹, Mingmin CHEN², Jiao WANG¹, Jie YUAN³, Qianwei ZHANG¹,
and Kaijie YANG³

¹ College of Energy & Power Engineering, Jiangsu University of Science and Technology, China

² College of Power and Energy Engineering, Harbin Engineering University, China

³ College of Aerospace Engineering, Nanjing University of Aeronautics and Astronautics, China

Abstract. In response to the problems of high-temperature gas intrusion and ablation in the expansion slit between ceramic tiles under complex flow conditions in the floating-wall combustion chamber, as well as the issue of hooks exceeding their service temperature, numerical simulations and analysis were conducted for this paper. The study revealed the mechanisms of gas intrusion and sealing and proposed two evaluation metrics for evaluating the cooling effect: the maximum temperature of the hook and the proportion of high-temperature area on the sidewall of the tile. Furthermore, the CRITIC weighting method was used to analyze the weight of these metrics. Based on this, the spacing, radius, and length effects on sealing and cooling effectiveness were studied, and multi-parameter calculations and optimization were performed. The results showed that the degree of gas intrusion in the transverse slit was significantly higher than that in the longitudinal slit. In addition, the sealing method of the jet impingement could effectively cool the downstream of both the transverse and longitudinal slit. The spacing of the jet impingement holes had the greatest impact on the cooling effect, followed by the radius and length. Finally, when the spacing of the holes is 10 mm, the length is 18.125 mm, and the radius is 1.6 mm, the cooling effect is optimal, with the proportion of high-temperature area on the side wall of the tile being 20.86% and the highest temperature of the hook reaching 836.02 K.

Keywords: gas turbine; floating-wall combustion chamber; gas intrusion; jet impingement cooling; CRITIC weighting.

1. INTRODUCTION

In the high-temperature and high-pressure working environment of gas turbines, the metal shell of the combustion chamber is susceptible to overheating [1], leading to thermal deformation and burn-through accidents [2]. To address this issue, ceramic tiles are commonly used to insulate the metal shell of the combustion chamber [3,4]. Presently, the floating-wall combustion chamber technology has been extensively researched and implemented, which involves creating narrow channels between insulation tiles and injecting cooling gas to prevent high-temperature gas infiltration. This technology boasts low cooling gas consumption and minimal temperature gradient on the wall, making it the primary structural form of combustion chambers. However, the structure and placement of jet impingement holes can significantly impact cooling efficiency [5]. Therefore, determining suitable parameters for the jet impingement holes is of urgent engineering significance for ensuring the safety of the insulation structure and improving the wall cooling efficiency of the combustion chamber.

Extensive research has been conducted by domestic and foreign experts and scholars on the issue of gas intrusion, mainly focusing on the mechanism of gas intrusion in the areas of the

rim of the compressor, rotors, and stators in the front end of the combustion chamber. Owen [6,7] proposed the mechanism of gas intrusion based on experimental results, which generally divides gas intrusion into outer-ring-induced intrusion, rotation-induced intrusion, and combined-induced intrusion. Jia *et al.* [8] studied the interaction mechanism between different sealing and cooling gas flows in the gap between the rotor-stator cavity and the slit, and the mainstream intrusion and obtained the conclusion that the sealing and cooling gas flow velocity has a significant effect on the sealing effect. The above scholars have conducted multi-angle research on the phenomenon of gas intrusion in the combustion chamber, but there have been few studies on the gas intrusion phenomenon and its sealing technology associated with the floating-wall combustion chamber and tile-hook structure.

Current research into combustion chambers has mainly focused on the cooling of the combustor liner and impingement/effusion cooling system. Andreini *et al.* [9] investigated two types of shock/jet structures through simulations and experiments. The results showed that the interaction of jets in a sparsely arranged array was weaker, while in a densely arranged array, there were strong secondary peaks and complex heat transfer modes, which were greatly influenced by the sparsity of the geometric structure on the recirculation of the cooling airflow. Jackowski *et al.* [10] investigated the cooling effect of different cavity heights and hole arrangements on the double-layer wall combustion chamber under multiple blowing ratios through experiments and obtained the local wall heat flux through sim-

*e-mail: shihong@nuaa.edu.cn

Manuscript submitted 2023-05-17, revised 2023-09-28, initially accepted for publication 2023-11-13, published in March 2024.

ulations. The study showed that the cooling effect was mainly influenced by the cold gas coverage of the outflow and the impact of shock cooling on the results was small. Kim *et al.* [11] designed an impingement/effusion cooling system that realizes the lowest thermal stress by using a second-order response surface method. Ahmed *et al.* [12] found that an optimum spreading hole spacing exists. Also, the minimum cooling effectiveness on the liner wall was found to be downstream of the impingement location. Ali *et al.* [13] optimized the liner cooling system and found that adding cooling holes to the inlet section would reduce the liner temperature but increase the combustion chamber outlet temperature. Wang *et al.* [14] investigated the cooling effect of different hole inclination angles and found that the cooling effect was best at 30°. Da Soghe *et al.* [15] explored the effect of the wall-to-jets temperature ratio on heat transfer. Liu [16–18] proposed two three-stage shock concepts that can effectively reduce cooling air consumption. The studies above did not cover the issues of gas intrusion and sealing of the slit located at the edge of the tile. Therefore, it is necessary to explore research on the edge slit of ceramic tiles, especially regarding the typical tile-hook structure, and investigate the temperature of the tile side wall and hook, as well as the optimization space of the jet impingement holes.

This paper investigates the typical tile-hook structure as the object of research and uses computational fluid dynamics simulation techniques to study the flow and mixing of cooling air and high-temperature combustion gas in the tile slit. The mechanism of gas intrusion and sealing in this structure is clarified based on the simulation results. Furthermore, two evaluation metrics are proposed to assess the cooling effect of the jet impingement holes, and their weights are analyzed. Finally, the jet impingement holes are subjected to multi-parameter calculations and optimization, resulting in the determination of optimal hole structure parameters that meet the requirements.

2. RESEARCH METHODS

2.1. Cooling mechanism

The combustion chamber investigated in this paper is a floating-wall combustion chamber of the gas turbine. The internal thermal protection as shown in Fig. 1 is mainly achieved by fixing ceramic tiles to the inner wall of the combustion chamber metal cylinder through hooks, which separates the internal flow field from the cylinder structure and avoids excessively high temperatures on the metal outer cylinder.

As the high-temperature gases sweep through the slit between the ceramic tiles, a portion of the gas separates and intrudes

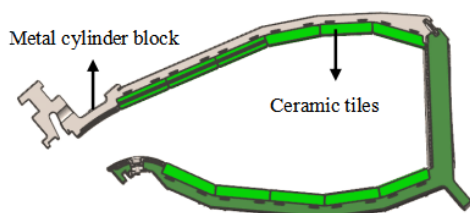


Fig. 1. Structural arrangement of tiles and hooks

into the slit due to the wall boundary layer and the Coanda effect [19]. Long-term exposure of ceramic tile side walls to high-temperature gas can cause ablation, and the high thermal conductivity of the metal hooks imposes more stringent temperature requirements. Therefore, an external cold flow is introduced to cool the components and seal off gas intrusion. As shown in Fig. 2, the cooling gas fills the outside of the metal casing and impacts the hooks from the jet impingement holes. Then it surges into the slit through the clearance between the hooks and the bottom of the casing and enters the pillow-shaped cavity, where it impacts and envelops the hooks, and collides and mixes with the invading high-temperature gas. Based on the cooling mechanism described above, this scheme can effectively reduce the temperature of the metal hooks and ceramic tiles while playing a sealing role to prevent high-temperature gas intrusion.

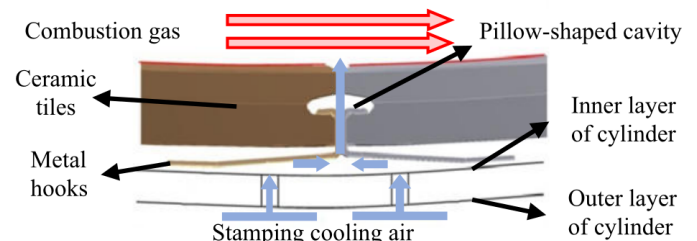


Fig. 2. Gas intrusion sealing mechanism

2.2. Physical modelling

This paper focuses on the tile configuration of the cross-shaped slit with the most distribution in the floating-wall combustion chamber, and a simplified model structure is shown in Fig. 3.

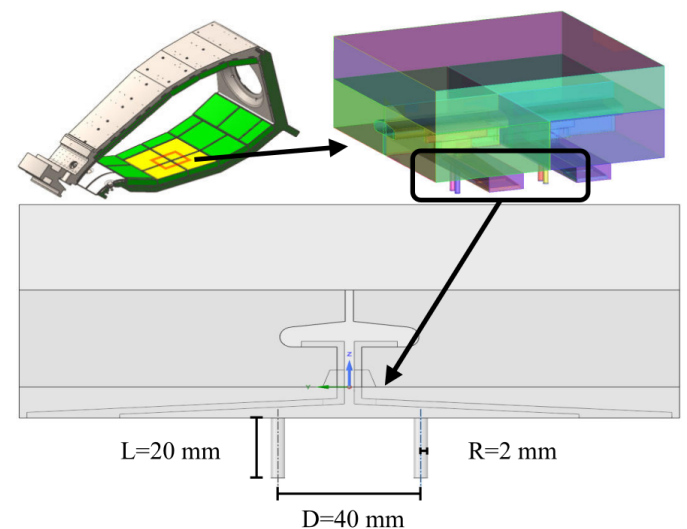


Fig. 3. Modelling and simplification of tile structures with cross slit

As shown in Fig. 3, the model includes a transverse slit (parallel to the hook) and a longitudinal slit (perpendicular to the hook), with pillow-shaped cavities running through the entire longitudinal slit, and two pairs of symmetrical jet impingement holes.

2.3. Boundary conditions

The structural elements and boundary conditions mentioned above are defined and numbered as shown in Fig. 4 and Fig. 5.

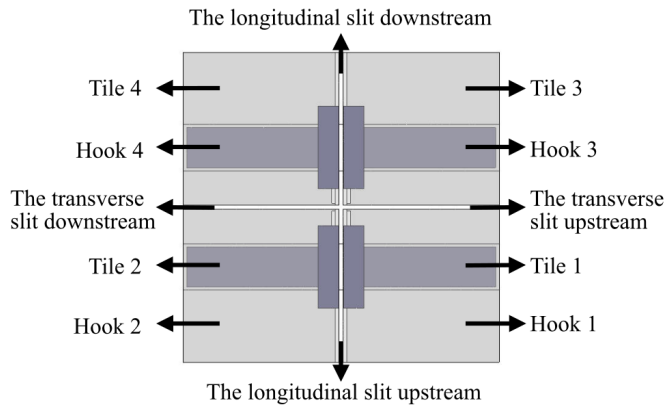


Fig. 4. Definition of the structure of the model

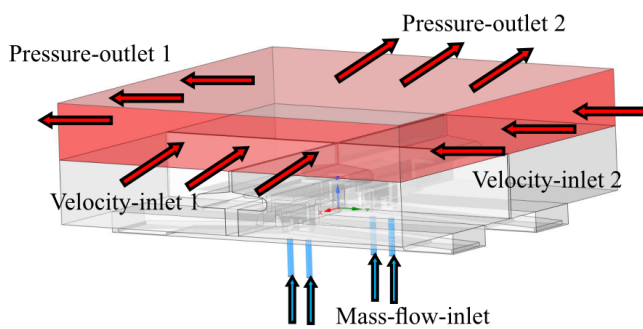


Fig. 5. Setting of the boundary conditions

The numerical simulation adopted boundary conditions based on the actual operating conditions of the combustion chamber, as shown in Table 1.

Table 1

Initial boundary conditions of the combustion chamber

Parameter terms for boundary conditions	Numerical values
High-temperature gas inlet velocity 1	30 m/s
High-temperature gas inlet temperature 1	1550 K
Outlet pressure 1	30 000 Pa
High-temperature gas inlet velocity 2	25 m/s
High-temperature gas inlet temperature 2	1500 K
Outlet pressure 2	27 000 Pa
Single cooling jet inlet mass flow rate	0.0042 kg/s
Cooling jet temperature	700 K
Environmental pressure	1 900 000 Pa

2.4. Evaluation metrics

Compared to ceramic tiles, the heat resistance of metal hooks is poor and they cannot withstand the intrusion of high-temperature mainstream gases. Once the service temperature is exceeded, it is highly likely to cause tile shaking and detachment, leading to a series of secondary accidents. Therefore, the maximum surface temperature of the metal hook under working conditions is one of the key factors determining whether the combustion chamber can operate stably. In addition, the researchers found that although ceramic tiles can withstand high temperatures, the temperature difference between the upper and lower surfaces of the tile sidewalls is large. If it is continuously and extensively in a high-temperature difference state, uneven heating will cause local ablation on the sidewall surface of the tile. The abnormal pores caused by ablation will damage the overall flowability of the combustion chamber and may exacerbate the degree of gas intrusion. Therefore, the evaluation metrics for the gas intrusion characteristics studied in this paper are the maximum temperature of the hook (T_h) and the proportion of the high-temperature area on the sidewall of the tile (P_t). According to the actual requirements of this type of gas turbine, the critical temperature of the sidewall of the tile is 1300 K, and the smaller the proportion of high-temperature areas, the better. The maximum service temperature of the metal hook is 850 K, and if it exceeds this standard, it is considered that the cooling effect has not met the requirements. The formula used in this paper to evaluate the ratio of the high-temperature area on the sidewall of the tile to the whole area is as follows:

$$P_t = \frac{S_c}{S}. \quad (1)$$

In equation (1), P_t represents the proportion of the high-temperature area, S represents the total area of the sidewall, and S_c represents the area of the sidewall where the temperature exceeds the critical temperature.

2.5. Algorithm validation

In this study, the standard $k-\varepsilon$ model equations were used to close the time-averaged continuity and momentum conservation equations [20], as this model has shown good robustness and performance in solving flow problems at high Reynolds numbers. To validate the reliability of our simulation algorithm, we conducted a verification based on the work of Bai *et al.* [21]. The experimental system schematic is shown in Fig. 6. This validation was simulated numerically using the boundary conditions specified in the literature. The numerical simulation results were compared with the experimental data by analyzing the effect of pitch variation on the cooling efficiency as shown in Fig. 7.

From the numerical simulation calculation results combined with the experimental data in Fig. 7, the cooling efficiency of the numerical simulation is slightly higher, but both have the same trend of variation with an error of no more than 3%. The main reason for this is that the experiment cannot achieve a completely uniform inlet. The experimental instrumentation also has errors arising from measurement accuracy, and components such as thermocouples can also produce flow resistance. Therefore, the

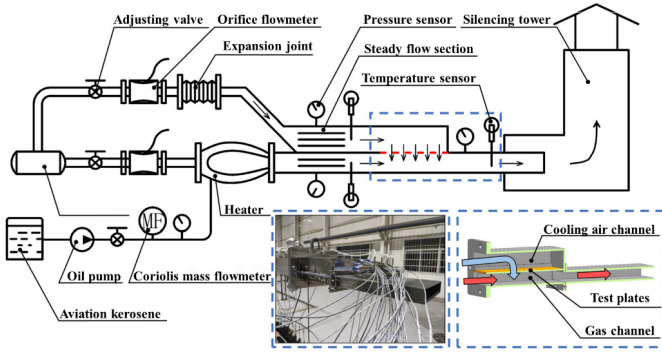


Fig. 6. Experimental schematic [21]

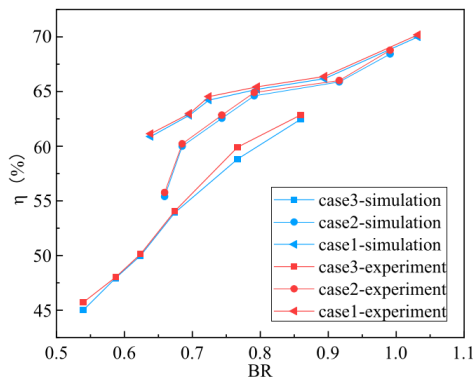


Fig. 7. Comparison of experimental and simulation conditions

experimental cooling efficiency is slightly lower than the results of the numerical simulation. In summary, the present method has a certain reference value for the simulation of the flow field of the tile slit in the combustion chamber and can be used for subsequent research and analysis.

2.6. Mesh independence validation

Prior to conducting numerical simulations of gas intrusion in the combustion chamber, we performed mesh independence verification. Initial target mesh sizes were set at 3.16 million, 3.88 million, 5.57 million, 7.31 million, and 9.69 million, respectively. As shown in Fig. 8, it can be observed that the T_h value

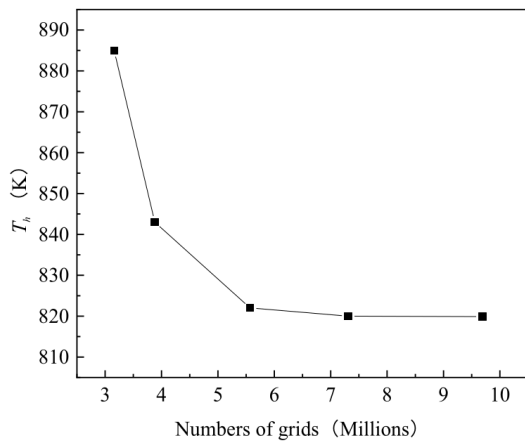


Fig. 8. Diagram of grid numerical validation results

stabilizes when the grid size exceeds 5.57 million, with no significant variation as the grid size further increases. Hence, considering grid density and computational resources, we opted to set the grid size at 5.57 million. Figure 9 illustrates the grids employed in this study. We refined the grids in regions with noticeable flow fluctuations to ensure that the $y+$ range remains within 25.5 to 34.9.

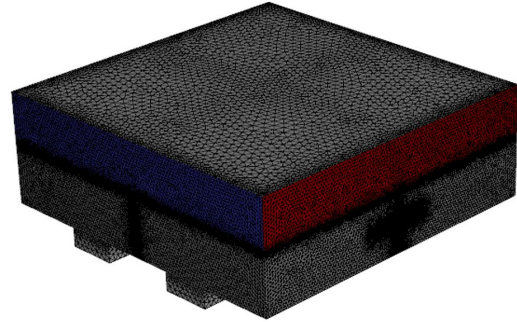


Fig. 9. Schematic of mesh

3. RESULTS AND DISCUSSION

Figure 10 shows schematic diagrams of the monitoring surfaces in the transverse and longitudinal slits of the tile, respectively, along with the corresponding temperature distribution.

As shown in Fig. 10, under the specified boundary conditions, the intrusion of high-temperature gas into the transverse slit is much greater than that into the longitudinal slit. As shown in Fig. 10c, the upstream part of the transverse slit exhibits severe gas intrusion, with high-temperature gas almost completely occupying this area, resulting in temperatures exceeding the critical temperature. The downstream high-temperature zones of the transverse slit are primarily located at the bottom and upper regions of the pillow-shaped cavity. As shown in Fig. 10d, the gas intrusion is more severe at the intersection of the two slits in the middle of the longitudinal slit, resulting in a significant temperature rise. Additionally, the temperature of the downstream edge is higher, and there is a tendency for high-temperature gas intrusion at the top of the upstream. Meanwhile, cold flow spills over from the top downstream of the slit, impacting the high-temperature gas and forming a gas film that provides excellent cooling effects for the downstream tiles. Figure 11 shows the velocity vectors on the middle monitoring surface of the tile slit.

As shown in Fig. 11a, under the influence of the Coanda effect and accompanied by the Venturi effect, a severe gas intrusion phenomenon occurred upstream of the transverse slit, where a large amount of high-temperature gas poured into the region at high speed. As a result of viscous shear, a vortex zone with high temperature and low velocity is formed at the edges. The high-temperature intrusion gas flowing through the transverse slit will be split up and down due to a large amount of cooling gas pooling in the central pillow-shaped cavity, with most of it moving in the direction of the bottom of the transverse slit along the tangent line and forming a vortex zone downstream. Meanwhile, a small part of it collides with the cold gas mass and then splits and intrudes into the top area of the downstream tile.

Optimization sealing and cooling to control gas intrusion in a floating-wall combustion chamber

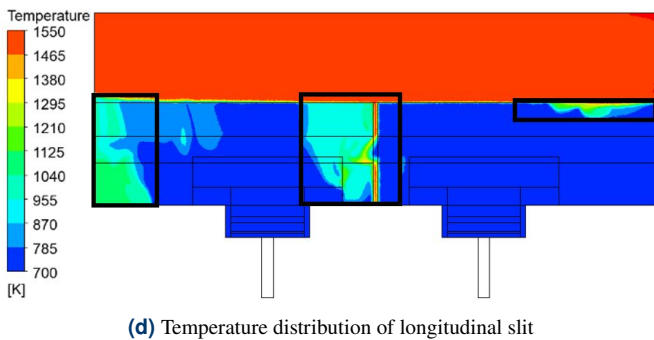
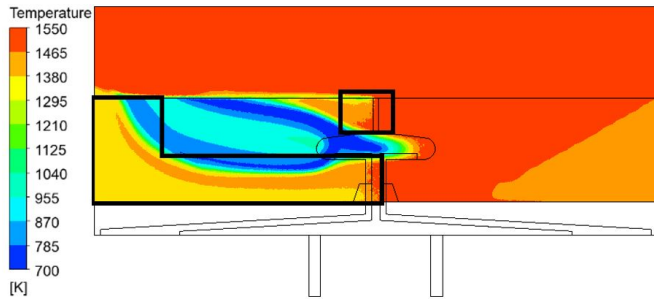
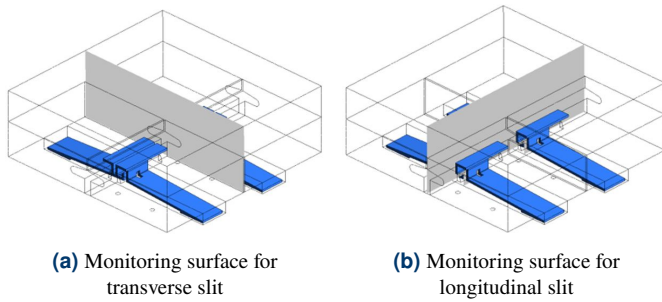


Fig. 10. Temperature distribution on the monitoring surface

Combined with Fig. 10c, it can be observed that the stratified flow of high-temperature gas and inadequate heat exchange with the cold flow are the main reasons for the significant temperature zoning downstream of the transverse slit.

As shown in Fig. 11b, the overall temperature of the longitudinal slit is observed to be lower due to the cold flow being the first to enter the longitudinal slit after impacting the hook, which allows the area to be sufficiently cooled. Furthermore, a large amount of cold flow rushes upwards at a higher velocity, hindering the main flow from entering and mixing with the small amount of invading high-temperature gas. The presence of the pillow-shaped cavity also provides favorable conditions for the cold flow to build up and fully exchange heat. It is worth noting that, as shown in Fig. 10d, a large vortex area is observed downstream of the longitudinal slit, where the cold flow does not flow sufficiently through the edge area, leading to poor heat transfer. In contrast, the flow field upstream of the longitudinal slit is more diffuse, with multiple vortices. Although the overall heat transfer effect is good, the cold flow is not uniformly distributed, which allows a small amount of high-temperature gas intrusion to occur at the top.

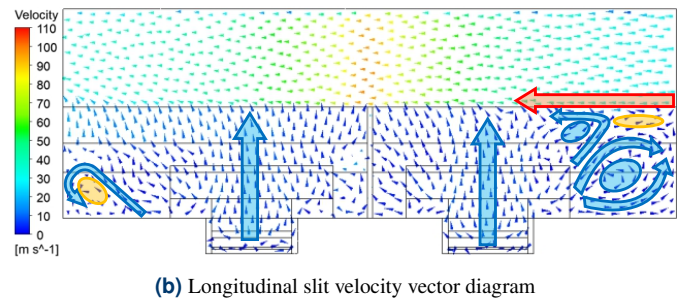
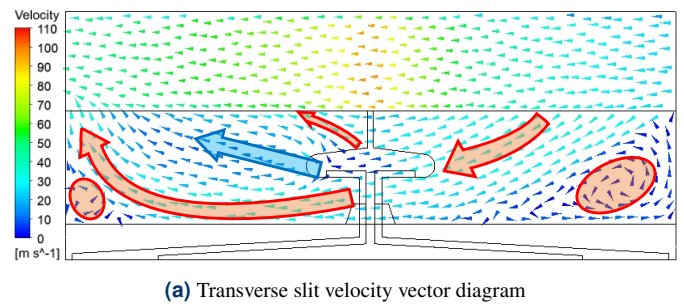


Fig. 11. Velocity vector distribution on the monitoring surface

The gas intrusion mechanism above directly leads to the overtemperature phenomenon on the tile sidewall surface and the hooks. Figure 12 and Fig. 13 show the temperature distribution on the tile sidewall surface and the hooks.

As shown in Fig. 12, both tile 1 and tile 4 have one side wall surface completely exceeding the critical temperature, and tile 2 and tile 3 side wall surfaces also have some areas exceeding

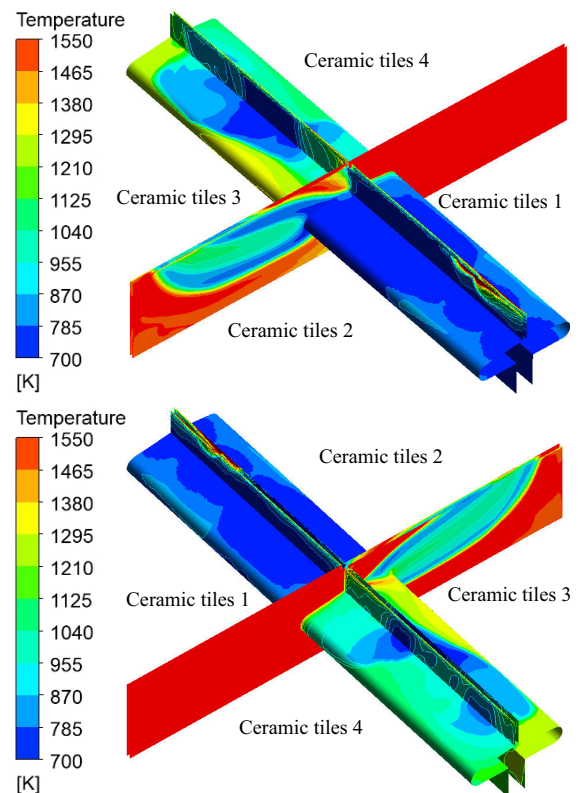


Fig. 12. Temperature distribution on the side walls of the tiles

H. Shi, R. Wang, M. Chen, J. Wang, J. Yuan, Q. Zhang, and K. Yang

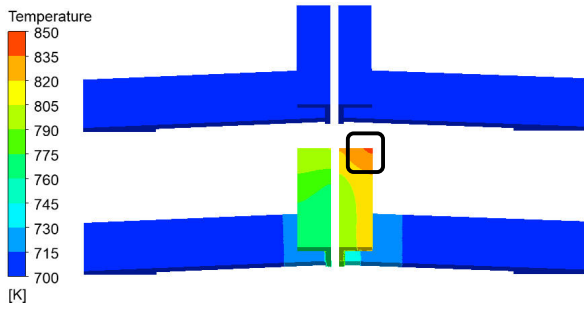


Fig. 13. Temperature distribution on the hooks

the critical temperature, with P_t reaching 23.79%. As can be seen from Fig. 13, T_h reached 850.81 K, which exceeded the service temperature. The over-temperature area is concentrated in one corner of hook 3 because hook 3 is downstream of the high-temperature mainstream sweeping direction, and part of the high-temperature gas intruded in the middle of the transverse slit retains its original flow direction, which directly impacts the edge of hook 3 downstream and makes it exceed the service temperature.

4. OPTIMIZATION

Although many works of literature point out that increasing the ram air flow can improve gas intrusion, this approach requires additional energy costs. Therefore, this paper proposes a cost-effective optimization scheme, which is a multi-parameter integrated optimization of the spacing, radius, and length of the jet impingement holes.

4.1. Spacing

Figure 14 shows the effect of the variation of the jet impingement hole spacing on P_t and T_h .

As can be seen from Fig. 14, T_h decreases linearly from 852.51 K to 836.5 K for the spacing of the jet impingement holes from 10 mm to 20 mm, while P_t increases linearly from 23.61% to 26.02%. T_h increases to 850.81 K at a pitch of 20 mm to 40 mm, while P_t decreases to 23.79%. The center axis surface of hooks 3 and 4 were monitored and the velocity vector distribution was observed, as shown in Fig. 15.

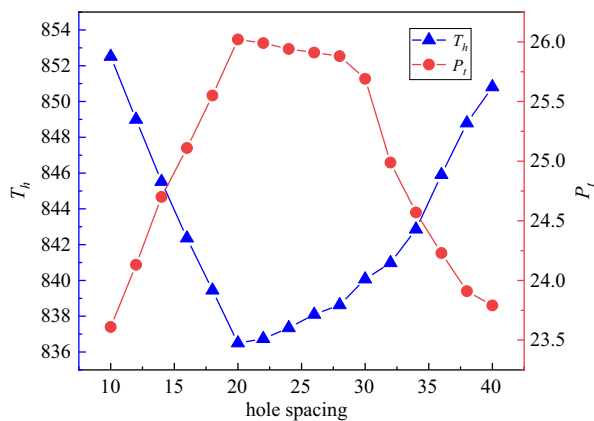
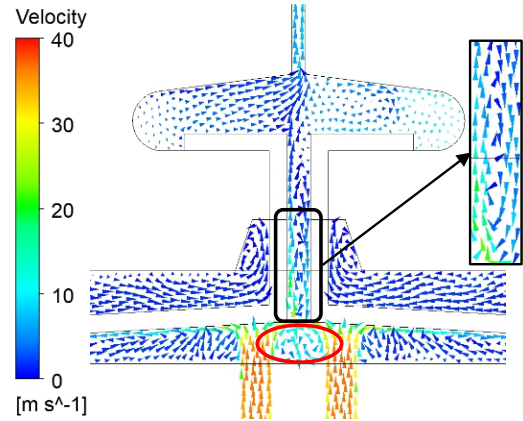
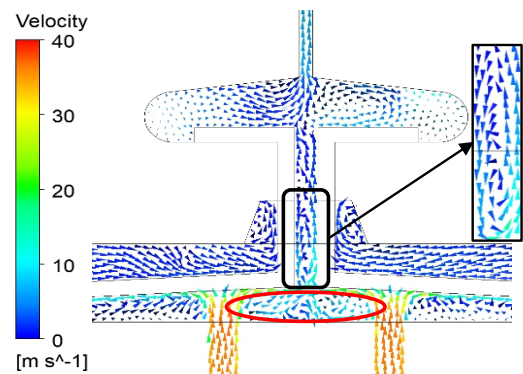


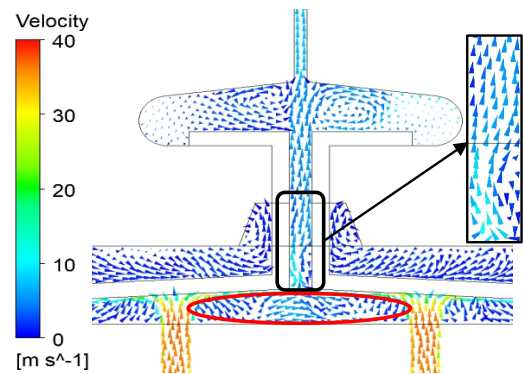
Fig. 14. Effect of spacing variation on structural temperature



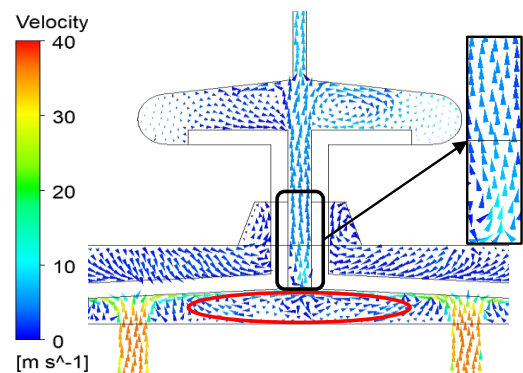
(a) Spacing of 10 mm



(b) Spacing of 20 mm



(c) Spacing of 30 mm



(d) Spacing of 40 mm

Fig. 15. Cross section of hooks 3 and 4 Velocity vector distribution

According to Fig. 15a and Fig. 15b, a vortex structure with high heat transfer capacity is formed at the bottom of the longitudinal slit of the tile when the spacing of the jet impingement holes is between 10 mm and 20 mm. The smaller the spacing of the holes, the higher the flow rate and therefore the lower the T_h . However, the formation of the vortex in the slit prevents the cold flow from spreading in all directions, so the cold air obtained from the transverse slit where the gas intrusion is severe decreases, leading to a gradual increase of P_t .

In contrast, according to Fig. 15c and Fig. 15d, when the spacing is expanded to more than 20 mm, the wall jet at the bottom of the hook develops uniformly in all directions, the two vortex structures at the bottom of the hooks are destroyed, and the overall flow field is changed considerably, so P_t and T_h no longer change linearly. With the continuous expansion of the jet impingement hole spacing, the flow field in the slit is gradually regularized, and the low-temperature vortex accumulated around the hook is gradually weakened, so the T_h gradually increases. In addition, in the area near the transverse slit, more cold flow is absorbed by the higher velocity transverse slit because the higher velocity transverse slit invades the heat flow and doping and cooling occurs, so P_t decreases.

4.2. Radius

Figure 16 shows the effect of radius variation on P_t and T_h .

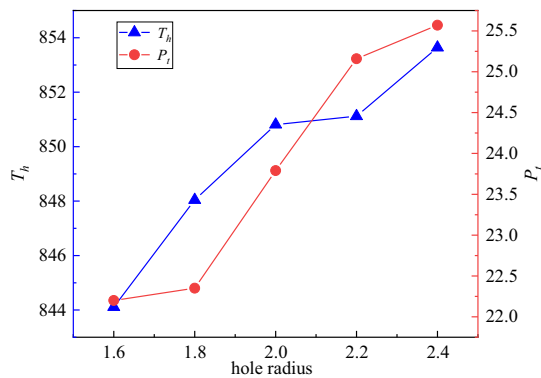


Fig. 16. Variation in temperature and flow rate at different radius

As can be seen in Fig. 16, when the radius of the jet impingement holes is increased from 1.6 mm to 2.4 mm, P_t increases from 22.2% to 25.57%, and T_h increases from 844.11 K to 853.64 K. The reason for the above phenomenon is that since the jet impingement holes are constant mass flow inlet, increasing the radius will reduce the outflow velocity and weaken the vortex strength in the flow field and the impact capacity of the wall-mounted jet, thus reducing the heat transfer capacity of the entire slit.

4.3. Length

Figure 17 shows the effect of the change in the length of the jet impingement holes on P_t and T_h .

As can be seen in Fig. 17, with the increase of length from 5 mm to 20 mm, P_t decreases from 25.52% to 23.79%, while T_h increases from 846.34 K to 850.81 K. Figure 18 shows

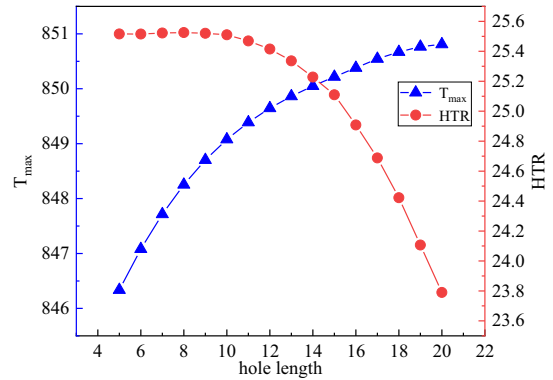


Fig. 17. Variation in temperature and flow rate at different lengths

the velocity vector distribution on the middle axis surface of hooks 3 and 4.

As shown in Fig. 18, the vortex structures gradually weaken and disappear as the length of the hole is reduced from 20 mm to 5 mm. A shorter hole length results in less along-travel loss and greater exit velocity, which reduces the strength of the vortex. Although this results in a slightly higher T_h , it also results in

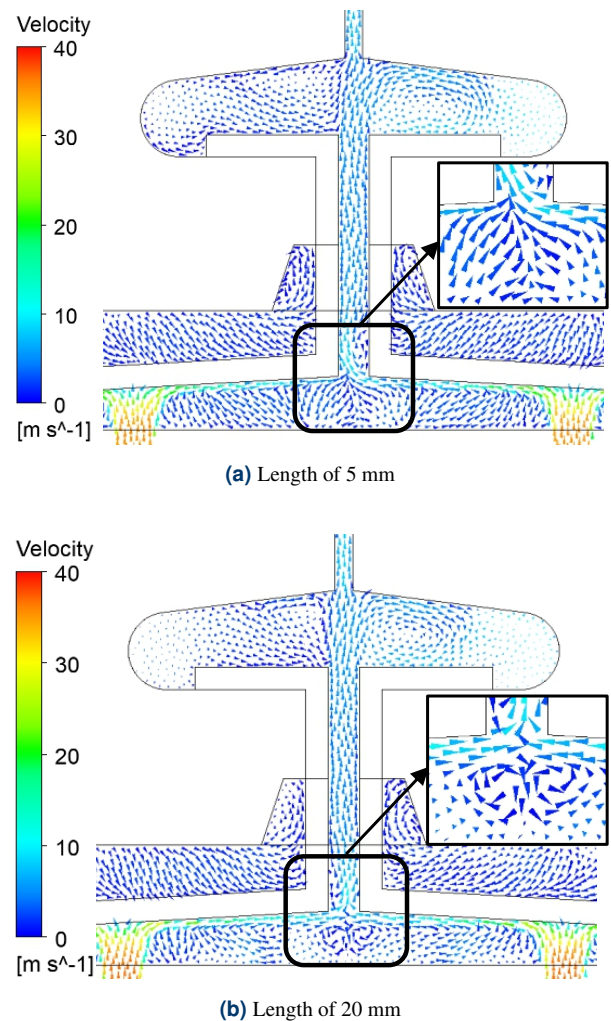


Fig. 18. Cross section of hooks 3 and 4 velocity vector distribution

better development of the slit flow field, which in turn wraps and directs more cold flow into the slit, thus reducing P_t .

Therefore, the flow field of the slit and the temperature of the tile-hook structure are influenced by multiple factors, including spacing, radius, and length of the jet impingement holes. Considering these factors together, conducting a comprehensive evaluation and finding the best for both evaluation matrixes under multiple objectives is necessary.

4.4. Integrated optimization based on the CRITIC weighting method

In this paper, a total of 72 feature structures in the spacing range of 10 mm–40 mm, the radius range of 1.6 mm–2.4 mm, and the length range of 5 mm–20 mm were selected for the calculation of the jet impingement holes. To further increase the number of samples and improve the optimization-seeking accuracy, the genetic aggregation algorithm in WORKBENCH response surface analysis was used to predict the data, and finally, 2500 sets of calculation results for different structures were obtained. In the following section, the CRITIC weighting method will be used to analyze the weights of two evaluation metrics.

The CRITIC weighting method is an objective weight assignment method proposed by DIAKOULAKI. It utilizes the variability and conflict of evaluation metrics to comprehensively measure the objective weight of metrics [22]. This method is particularly suitable for multi-attribute and multi-objective decision-making scenarios. The steps of the integrated model construction of the CRITIC weighting method are as follows:

1. Assuming there are n samples to be evaluated and m evaluation metrics, a raw data matrix of the evaluation metrics is formed:

$$X = \begin{bmatrix} x_{11} & \cdots & x_{1m} \\ \vdots & \ddots & \vdots \\ x_{n1} & \cdots & x_{nm} \end{bmatrix}. \quad (2)$$

The notation x_{ij} represents the value of the j th evaluation metric for the i th sample in the original data matrix, which consists of n samples and m evaluation metrics.

2. Since this article focuses on the percentage of high temperature on the side wall of the tile and the highest temperature value of the hook, smaller values are better, and the dimensions are different. Therefore, the original matrix is reversed and normalized:

$$x'_{ij} = \frac{x_{\max} - x_j}{x_{\max} - x_{\min}}. \quad (3)$$

3. The variability of matrices is expressed in the form of standard deviation:

$$\begin{cases} \bar{x}_j = \frac{1}{n} \sum_{i=1}^n x_{ij}, \\ S_j = \sqrt{\frac{\sum_{i=1}^n (x_{ij} - \bar{x}_j)^2}{n-1}} \end{cases} \quad (4)$$

where S_j shows the standard deviation of the j th matrix.

4. Conflict of matrices is expressed by correlation coefficient:

$$R_j = \sum_{i=1}^p (1 - r_{ij}), \quad (5)$$

where r_{ij} denotes the correlation coefficient between evaluation matrices i and j .

5. Amount of information:

$$C_j = S_j \sum_{i=1}^p (1 - r_{ij}) = S_j \times R_j, \quad (6)$$

where the larger C_j is, the greater the role of the j th evaluation matrix in the overall evaluation matrix system, and the more weight should be assigned to it.

6. Objective weights:

In summary, the objective weights W_j of the j -th matrix are:

$$W_j = \frac{C_j}{\sum_{j=1}^p C_j}. \quad (7)$$

The high-temperature proportion of the tile sidewall surface and the maximum temperature weighting of the hooks are shown in Table 2.

As can be seen from Table 2, the weight of P_t is 57.53%, which is higher than the weight of 42.47% accounted for by T_h . Found the optimal structural parameters on this basis, due to the limitation of space, this paper takes the top 5 and last 5 solutions as examples, and the specific optimization results are shown in Table 3.

As can be seen from Table 3, the result of the No. 1 scheme has the highest overall score of 0.89746. The P_t accounts for 20.86% and T_h is 836.02 K, which meets the design requirements. Correspondingly, the jet impingement hole spacing is

Table 2
Results of the weighting calculation

Object	Sample size	Average value	Standard deviation	Variability of metrics	Conflict of metrics	Volume of information	Weight
T_h (K)	2500	0.563	0.168	0.168	1.305	0.220	42.47%
P_t (%)	2500	0.368	0.228	0.228	1.305	0.298	57.53%

Table 3
Optimization results

Number	Composite score	P_t (%)	T_h (K)
1	0.89746	20.861	836.016
2	0.89729	20.821	836.409
3	0.89365	20.929	835.693
4	0.89276	20.813	836.862
5	0.88663	21.018	835.449
2496	0.20420	25.288	852.655
2497	0.20049	25.217	853.640
2498	0.19895	25.545	850.682
2499	0.19877	25.488	851.233
2500	0.19855	25.282	853.191

10 mm, the length is 18.125 mm and the radius is 1.6 mm. In this paper, numerical simulation is further developed to verify this solution and compare it with the initial structure, as shown in Figs. 19 and 20.

As can be seen from Fig. 19, after optimization, the over-temperature phenomenon downstream of the transverse slit was greatly relieved, and P_t was reduced to 21.03%. As can be seen

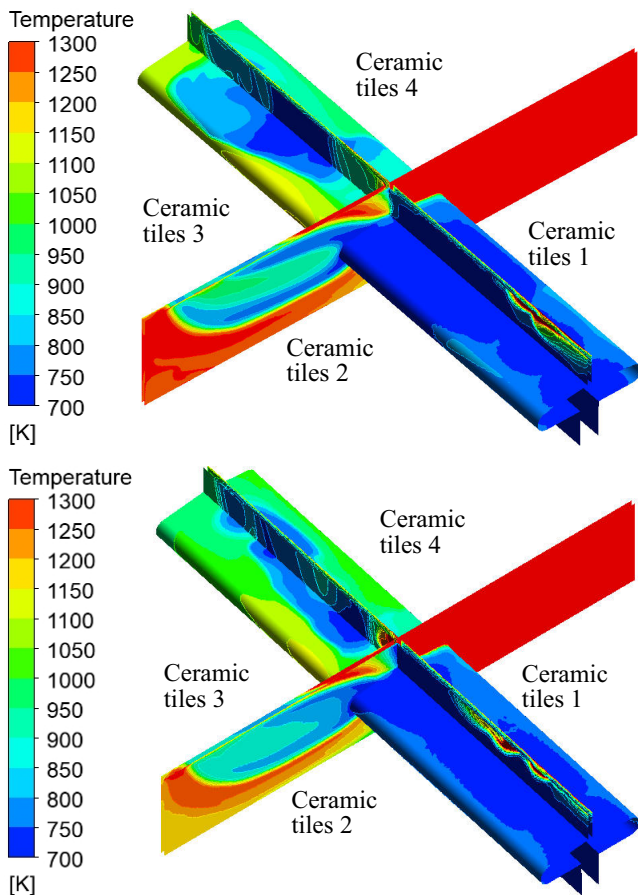


Fig. 19. Comparison of the temperature distribution on the side walls of the tiles

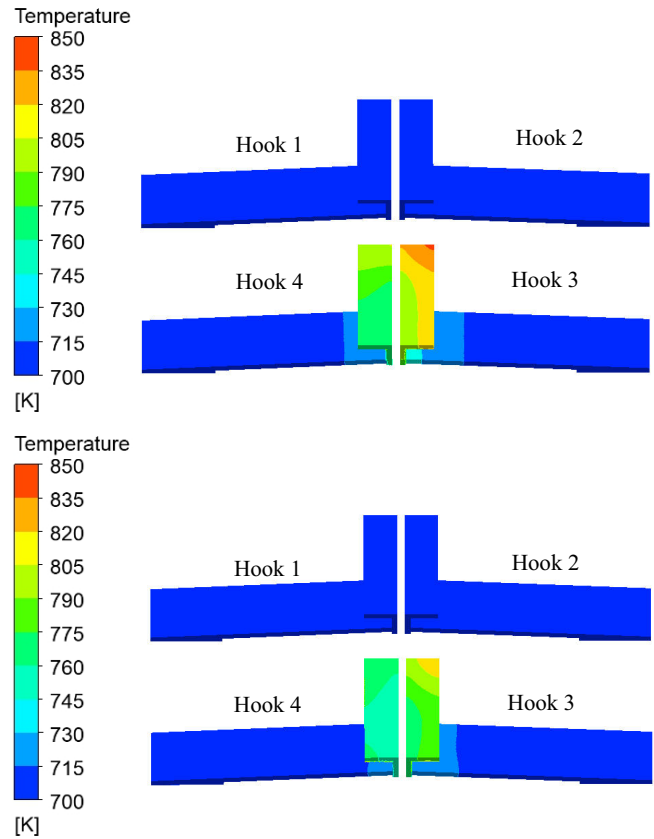


Fig. 20. Comparison of the surface temperature distribution of the hooks

from Fig. 20, the effect of temperature reduction of hook 3 and hook 4 is remarkable, and T_h of hook 3, which was originally over-temperature, has been reduced to 833.7 K, which has met the service requirements. It is verified that the error between the prediction result of the No. 1 scheme and the numerical simulation result is only 0.8%, which has high accuracy.

5. CONCLUSIONS

This paper investigates the arrangement and distribution characteristics of tiles and hooks in a floating-wall combustion chamber of a gas turbine and analyzes the gas intrusion mechanism of the typical tile hook at the cross-shaped slit. The temperature field distribution of the tile hook and the flow field characteristics of the slit are obtained, and the effects of the spacing, radius, and length of the jet impingement holes on the gas intrusion sealing performance are examined. The genetic aggregation algorithm is used to expand the sample capacity for prediction, and the CRITIC algorithm is employed for weight analysis and multi-objective optimization. Ultimately, a jet impingement hole structure with excellent gas intrusion sealing performance is obtained. The main findings are as follows:

1. For the ceramic tile sidewall surface and slit, the transverse slit is much more susceptible to gas intrusion than the longitudinal slit, and there's significant temperature zoning on downstream wall surfaces. The longitudinal slit is sufficiently cooled and more resistant to gas intrusion.

2. For the metal hooks, the T_h of hooks 3 and 4 is higher in the initial working condition, and the maximum difference with hooks 1 and 2 is above 30%. The main reason is that hooks 3 and 4 are in the mainstream sweeping direction and downstream of the transverse slit, and some of the gas intruding from the middle of the transverse slit still retains the original sweeping angle, resulting in impingement on hooks 3 and 4.
3. The spacing of the jet impingement holes has the most significant impact on the sealing and cooling effect, followed by the radius and length. The optimal solution has a spacing of 10 mm, a length of 18.125 mm, and a radius of 1.6 mm. Compared to the initial model, this solution reduces P_t from 23.79% to 21.03%, and T_h is reduced from 850.81 K to 833.7 K, which meets the service requirements. However, despite our optimization efforts, the transverse slit cooling performance still falls short of excellence. This is because the evaluation indicator we employed is a composite measure and cannot guarantee the optimization of every individual sub-criterion, such as the transverse slit cooling indicator.
4. The optimization process resulted in the identification of the ideal structural parameters for the holes that meet the requirements. Through this approach, the enhancement of both combustion chamber sealing and cooling is achieved while significantly reducing the need for extensive alterations to the overall structure, thus achieving higher feasibility.

REFERENCES

- [1] A.B. Ali, W. Kriaa, H. Mhiri, and P. Bournot, "Numerical investigations of cooling holes system role in the protection of the walls of a gas turbine combustion chamber," *Heat Mass Transf.*, vol. 48, no. 5, pp. 779–788, May 2012.
- [2] K.M. Kim, Y.H. Jeon, N. Yun, D.H. Lee, and H.H. Cho, "Thermomechanical life prediction for material lifetime improvement of an internal cooling system in a combustion liner," *Energy*, vol. 36, no. 2, pp. 942–949, Feb 2011.
- [3] P. Tarnawski and W. Ostapski, "Rotating combustion chambers as a key feature of effective timing of turbine engine working according to Humphrey cycle – CFD analysis," *Bull. Pol. Acad. Sci. Tech. Sci.*, vol. 70, no. 5, p. e143100, Oct 2022.
- [4] K. Chidambaram and T. Packirisamy, "Smart ceramic materials for homogeneous combustion in internal combustion engines – A review," *Therm. Sci.*, vol. 13, no. 3, pp. 153–163, 2009.
- [5] W.W. Choi and S.M. Kim, "Effect of effusion hole arrangement on jet array impingement heat transfer," *Int. J. Heat Mass Transf.*, vol. 192, p. 122900, Aug 2022.
- [6] J.M. Owen, "Prediction of Ingestion Through Turbine Rim Seals – Part I: Rotationally Induced Ingress," *J. Turbomach.-Trans. ASME*, vol. 133, no. 3, p. 031005, Jul 2011.
- [7] J.M. Owen, "Prediction of Ingestion Through Turbine Rim Seals-Part II: Externally Induced and Combined Ingress," *J. Turbomach.-Trans. ASME*, vol. 133, no. 3, p. 031006, Jul 2011.
- [8] X.Y. Jia, H.Y. Dong, Y.Z. Ming, Y. Wu, and L.D. He, "Hot gas ingestion in chute rim seal clearance of gas turbine," *Int. J. Turbo Jet-Engines*, vol. 40, no. 3, pp. 329–339, 2023, doi: 10.1515/tjj-2021-0010.
- [9] A. Andreini, L. Cocchi, B. Facchini, L. Mazzei, and A. Picchi, "Experimental and numerical investigation on the role of holes arrangement on the heat transfer in impingement/effusion cooling schemes," *Int. J. Heat Mass Transf.*, vol. 127, pp. 645–659, Dec 2018.
- [10] T. Jackowski, M. Elfner, and H.J. Bauer, "Experimental Study of Impingement Effusion-Cooled Double-Wall Combustor Liners: Thermal Analysis," *Energies*, vol. 14, no. 16, p. 4843, Aug 2021.
- [11] K.M. Kim, H. Moon, J.S. Park, and H.H. Cho, "Optimal design of impinging jets in an impingement/effusion cooling system," *Energy*, vol. 66, pp. 839–848, Mar 2014.
- [12] S. Ahmed, B.H. Wahls, S.V. Ekkad, H. Lee, and Y.H. Ho, "Effect of Spanwise Hole-to-Hole Spacing on Overall Cooling Effectiveness of Effusion Cooled Combustor Liners for a Swirl-Stabilized Can Combustor," *J. Turbomach.-Trans. ASME*, vol. 144, no. 7, p. 071015, Jul 2022.
- [13] A.B. Ali, W. Kriaa, H. Mhiri, and P. Bournot, "Analysis of the influence of cooling hole arrangement on the protection of a gas turbine combustor liner," *Meccanica*, vol. 53, no. 9, pp. 2257–2271, Jul 2018.
- [14] J. Wang, Z.W. Hu, C. Du, L. Tian, and J. Baleta, "Numerical study of effusion cooling of a gas turbine combustor liner," *Fuel*, vol. 29, p. 120578, Jun 2021.
- [15] R. Da Soghe, C. Bianchini, J. D'Errico, and L. Tarchi, "Effect of Temperature Ratio on Jet Impingement Heat Transfer in Active Clearance Control Systems," *J. Turbomach.-Trans. ASME*, vol. 141, no. 8, p. 081009, Aug 2019.
- [16] K.X. Liu, "Heat transfer characteristics of triple-stage impingement designs and their application for industrial gas turbine combustor liner cooling," *Int. J. Heat Mass Transf.*, vol. 172, p. 121174, Jun 2021.
- [17] K. Liu and Q. Zhang, "A Novel Multi-Stage Impingement Cooling Scheme – Part I: Concept Study," *J. Turbomach.-Trans. ASME*, vol. 142, no. 12, p. 121008, Dec 2020.
- [18] K. Liu and Q. Zhang, "A Novel Multi-Stage Impingement Cooling Scheme – Part II: Design Optimization," *J. Turbomach.-Trans. ASME*, vol. 142, no. 12, p. 121009, Dec 2020.
- [19] J.U. Choi, G.M. Kim, H.C. Lee, and J.S. Kwak, "Optimization of the Coanda bump to improve the film cooling effectiveness of an inclined slot," *Int. J. Therm. Sci.*, vol. 139, pp. 376–386, May 2019.
- [20] J. Joy, P.C. Wang, and S.C.M. Yu, "Effect of geometric modification on flow behaviour and performance of reverse flow combustor," *Proc. Inst. Mech. Eng. Part G-J. Aerosp. Eng.*, vol. 233, no. 4, pp. 1457–1471, Mar 2019.
- [21] N.J. Bai *et al.*, "Experimental investigations into the effusion plate wall temperature of impingement/effusion cooling systems for gas turbine combustors," *Aerosp. Sci. Technol.*, vol. 132, p. 108052, Jan 2023.
- [22] A.R. Krishnan, M.M. Kasim, R. Hamid, and M.F. Ghazali, "A Modified CRITIC Method to Estimate the Objective Weights of Decision Criteria," *Symmetry-Basel*, vol. 13, no. 6, p. 973, Jun 2021.